SOLPS simulations of EAST radiation divertor with N and Ar seeding

X.J. Liu[1,*], G. Deng[1], S. Liu, J. Huang[1], C. Wu[1], L. Zhang[1], X. Gao[1], and EAST Team[1]

[1]Institute of Plasma Physics, Chinese Academy of Sciences, P.O. 1126, 230031 Hefei, Anhui, China
*Eamil:julie1982@ipp.ac.cn

Abstract

A critical issue for EAST and future tokamak machines such as ITER and China Fusion Engineering Testing Reactor (CFETR) is the elimination of excessive heat load on the divertor target plates. As a means of actively reducing and controlling the power fluxes to the target plates, localized impurity (N, Ar) gas puffing from lower dome is investigated by using SOLPS5.0 on EAST with double null configuration. The radiative efficiency and distribution of the two gases are compared. The effect of N and Ar seeding on target power loading and the confinement is also presented. The simulation results indicate that both N and Ar puffing can effectively reduce the peak heat flux load and electron temperature Te at divertor targets similarly. N seeding can reach a higher radiative loss fraction (~85%) than Ar case (~75%), and N radiates power in divertor region mianly, while the radiative power inside separatrix for Ar seeding is also significant. Ar impurity puffing results in a faster decrease of the power across the sepatratrix, it seems unfavourable for plasma performance with the heating power close to the L-H transition threshold power.

Keywords: EAST, radiative divertor, SOLPS, impurity seeding

1. Introduction

The mitigation of divertor heat flux is an active topic of inverstigation on present tokamaks. It's also a critical issue for EAST to explore a long pulse and high heating power operation. This problem may become more crucial if carbon has to be avoided as a plasma facing material for ITER and China Fusion Engineering Testing Reactor (CFETR) due to high co-deposition of tritium [1]. One promising approach is seeding impurity gases with high radiative loss rate to enhance the radiation from both inside and outside the last closed flux surface (LCFS), to convert plasma thermal energy to radiation spread over a much larger surface area and eventually to reduce the target heat load. This technique has been investigated on a number of tokamaks in both L- and H-mode [2-5]. In order to optimize the choice and puffing rate of impurity seeded, detailed modeling and analysis is necessary to understand well the radiative distribution and their effect on heat load on divertor targets and core performance.

In this paper, we use the SOLPS5.0 code package [6] for the simulations of scrape-off layer (SOL) and divertor plasma. SOLPS mainly consists of two coupled codes: B2.5 is a fluid code that solves Braginskii-like equations for the ions (D, C, He, N, Ar) and electrons. Eirene is a Monte-Carlo code that describes kinetic neutrals [7]. Both codes are coupled via source terms for particle, momentum and energy. As we known, the atomic physics model and database are significant in determining the plasma constituents and the interaction among them. Since ADAS (Atomic Data and Analysis Structure) database [8] is actively maintained and upgraded, the mainly atomic processes included in this work, for example, ionization, excitation, dissociation, charge exchange and elastic collisions are from ADAS database. The accuracy of the data is mostly considered to be about 10-20%.

Detailed modeling studies of divertor target power loading and radiative distribution in EAST, as well as the consequence for core confinement with N and Ar seeding are presented by using SOLPS5.0. In section 2 we briefly describe the EAST divertor geometry and computational mesh, as well as the modeling setups. The modeling results and discussions with N and Ar seeding are presented in section 3, followed by a summary in section 4.

2. Simulation parameters

2.1. Geometry and computational grid

A grid is constructed for double null shot 41383 at 4.5 s shown as Fig. 1. Equilibrium is provided by equilibrium fitting (EFIT) code. The computational region includes the 'core' region (a small segment of the region with closed field lines, i.e., the area between core edge interface (CEI) and separatrix), left SOL region and right SOL and the private flux regions (PFR), including upper and lower PFR. The grid has 98 poloidal including the guard cells at four targets and 36 radial cells including the guard cells at the core and SOL boundaries, with the separatrix being located between cell number 18 and 19. It stretches radially from about -3.8 cm to 3.7 cm on either side of the separatrix at the midplane.

2.2. Boundary conditions and modeling assumptions

In modeling, the multi-fluid species includes D^0 neutrals, D^+ main ions and C impurities with neutral C^0 and all charged state ions and additional N^{0-7+} in N seeding case and Ar^{0-18+} instead in Ar seeding plasma. Carbon is produced self-consistently from physical and chemical sputtering and has zero recycling at targets, PFR, and SOL boundaries. The physical sputtering rates for both ions and neutrals are taken from the TRIM database [9]. Constant chemical sputtering rate 2% is used for carbon production. The transport of hydrocarbons is not included in this paper and the sputtered material and the seeded impurities (N and Ar) are treated as atom. The power across the CEI enter into the computational region is set to $P_{CEI} = 1.6$ MW, which is calculated according to the energy balance by subtraction of ~20% radiation power (=0.4 MW) inside the CEI surface not accounted in this simulations from the total heating power. It is equally distributed between electrons and ions. The density of bulk ions D^+ is set to 1.0×10^{19} m^{-3} at the outer midplane separatrix and maintained by a feedback loop through D_2 gas puffing outside the SOL region (see Fig. 1). Normally, the anomalous cross-field transport coefficients are determined by fitting the upstream density (n_e) and temperature (T_e) profiles measured by RP (Reciprocating Probe) and edge TS (Thomson Scattering) system. However the upstream profiles for n_e and T_e are not available for this discharge, so we choose a typical empirical value $D\perp = 0.3$ m^{2}s^{-1} and $\chi e = \chi_i = 1.0$ m^{2}s^{-1} for particle and ion and electron heat diffusivities respectively is this paper. The parallel plasma transport is flux limited, and no drifts are included in this simulation. The radial decay length λ_T for both electron and ion temperature and λ_n are set to 0.03 m. The recycling coefficients for D^0 and D^+ are set to 1.0 at the PFR and outer SOL edges. At the divertor target plates, the standard sheath boundary condition is applied. According to the Bohm criterion, the flow will be at least the sonic speed at the sheath entrance. The sheath heat transmission coefficients for electrons and ions are set to 4.5 and 2.5, respectively.
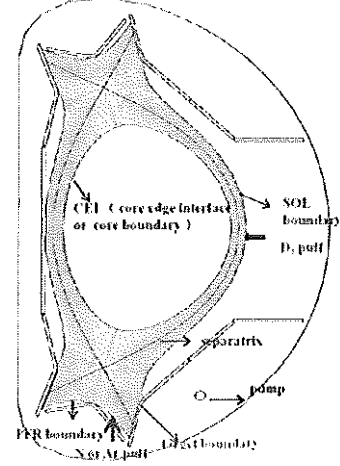

FIG 1. The 2D physical mesh for modeling in this paper is shown. The impurity gas (N and Ar) are injected from t h e lower dome and D_2 puffing for controlling the electron density at the outer midplane separatrix. The boundaries are pointed out with arrows.

3. Simulation results and discussions

3.1. The distribution of radiation power and its effect on divertor behavior

To detailed investigate the distribution and its effect on the heat flux load and temperature at divertor targets with N and Ar seeding, we have carried out an impurity puffing rate scan. The radiation power in edge including the SOL and divertor region ($P_{edge,rad} = P_{SOL,rad} + P_{div,rad}$), i.e., the whole area outside the separatrix and in core region which covers the entire area inside separatrix surface ($P_{core,rad} = 0.4MW + P_{core,SOLPS}$), as well as the peak electron temperature at lower outer divertor as a function of radiation power loss fraction (f_{rad}) for N and Ar seeding are shown in Fig. 2(a) and 2(b)
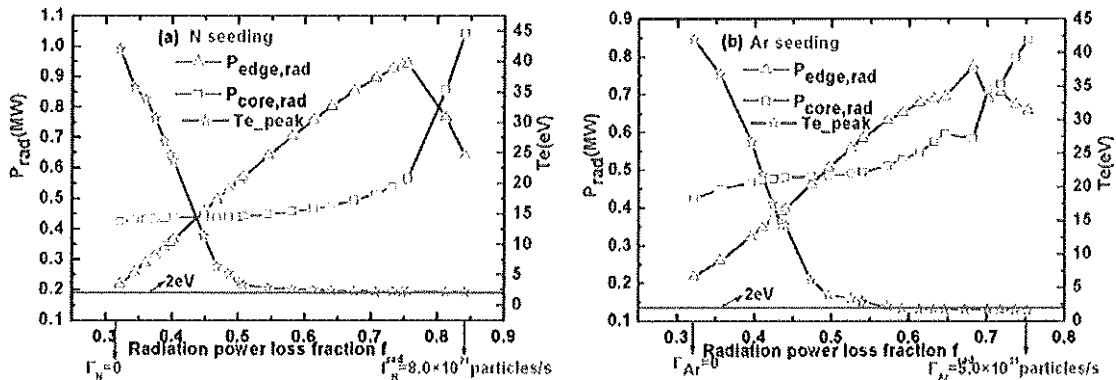

FIG 2. The radiation in edge (the whole area outside the separatrix) and in core region (including the radiation inside CEI surface), as well as the peak electron temperature at lower outer divertor against radiation power loss fraction for N seeding (a) and Ar seeding (b) are shown. The horizontal solid lines correspond to 2eV.

respectively. The horizontal solid lines correspond to 2eV. We can find that N seeding can reach a higher radiative loss fraction f_{rad} ~85% (corresponding to N puffing rate $\Gamma_N = 8.0 \times 10^{21}$ particles/s) than Ar seeding f_{rad} ~75% (with Ar puffing rate $\Gamma_{Ar} = 5.0 \times 10^{21}$ particles/s), and N radiates power in divertor region mianly, while the radiative power inside separatrix for Ar seeded discharge is also significant. For N seeding, $P_{edge,rad}$ increase as f_{rad} increasing and reach the maximum value at f_{rad} ~75%, while $P_{core,rad}$ is almost flat until f_{rad} >75%. When f_{rad} >75%,

the radiation power move into separatrix and exceed the radiative loss in edge at f_{rad}~80%. For Ar seeded case, both $P_{edge, rad}$ and $P_{core, rad}$ increase, and it increases faster in edge region than in core region when f_{rad}<65%, and the radiation in core region dominates when at f_{rad}>70%. Fig. 2 also shows that both N and Ar puffing can effectively reduce the peak electron temperature Te and heat flux load (not shown in Fig. 2) at divertor targets similarly. The divertor get detachment (Te_peak ~2eV) when the impurity gas puffing reach at a relatively high level of f_{rad}.

To make it clean, we plot the radiation power ratio of edge to core against f_{rad} with N and Ar seeding in Fig. 3. We can see that the ratio is totally higher for N seeding plasma than for Ar. It means that $P_{edge, rad}$ is higher for low-z N seeding than Ar. It also can be found that the ratio increases against f_{rad} and reach the maximum value, then drops for both N and Ar seeding, the maximum value reaches at f_{rad}~70% for N seeded and f_{rad}~60% for Ar. The ratio increases faster in N seeding plasma than in Ar case. It indicates that when seeding with N, the increased radiative power is mainly in edge region, while in Ar seeding case, power radiates in core region also significantly.

FIG 3. The radiative power ratio of edge to core is plotted as a function of radiation power loss fraction with N and Ar seeding.

3.2. The effect of impurity seeding on confinement

Beside the mitigation of divertor heat load, another crucial consideration for impurity seeding is to keep the compatibility with core performance. A strong positive correlation between normalized energy confinement factor H_{98} (which is an indicator of confinement) with the edge effective charge Zeff was found in [4, 10]. In Fig. 4, the effective charge at CEI (Z_{CEI}) as a function of the total radiative power fraction f_{rad} is illustrated. As can be seen, Z_{eff} at CEI is totally larger in N seeding than in Ar seeding at a fixed f_{rad}. We can deduce that N has a higher confinement than Ar from the relationship between H_{98} and Z_{eff} [10]. More detailed experimental validation on it will be performed in future. The results also show that Z_{eff} at CEI vary slightly with f_{rad} when f_{rad}<50%. It suggests that the divertor screening for impurities injected get weaker at a high level f_{rad}. The effect of different impurities seeding on the energy confinement has been investigated on experiments [2, 11]. The results show that H_{98} is to a large degree independent of radiating impurity when the power across the separatrix entering into SOL (P_{sep}) is larger than the threshold power of L-H mode transition (P_{th}). It means H_{98} depends strongly on the different between input power and the radiated power inside the LCFS. So we plot P_{sep} with N and Ar seeding case against the radiated fraction f_{rad} in Fig. 5. The horizontal solid line indicates the predicted L-H transition threshold power P_{th} (~1.55 MW) for this discharge by using the formula in [12], which is in proximity to P_{sep} without any impurity seeding of this simulated discharge. It appears that P_{sep} decreases faster with Ar seeding than N. It indicates that Ar is not a good radiator when the heating power is close to P_{th}, it may induces the degradation of H_{98}.

FIG 4. The effective charge at CEI against f_{rad} with N and Ar seeding.

3.3. Discussions

In fact, all the differences between N and Ar seeded plasma are attributed to their different radiation characteristics. Fig 6 shows the radiative power loss rate L_z of some important elements in tokamak plasma as a function of temperature at a fixed n_e (~$10^{20}m^{-3}$) calculated from the non-local thermodynamic equilibrium (NLTE) collisional radiative (CR) model by FLYCHK code [13].We can see that N radiation peak is at Te ~10-30eV, it's a good divertor radiator for EAST. The first radiation peak of Ar is almost at the same Te with N, and there is another higher radiation peak at Te ~ 100-500eV. That suggests Ar is a good radiator for both divertor and core region simultaneously, it may be suitable for ITER or DEMO to reduce the power enter into SOL region. We also can find that N has the similar L_z with C, it seems to be a C-like radiator. That would be the reason why N seeding can recover some or all the loss of H_{98} in metallic wall
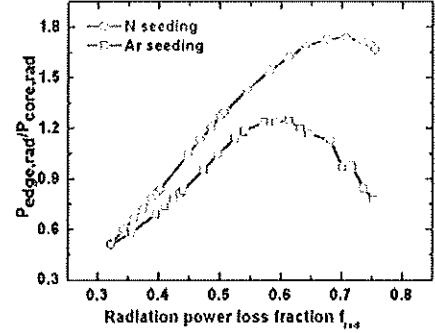

FIG 5. The radiative power ratio of edge to core is plotted as a function of radiation power loss fraction with N and Ar seeding.
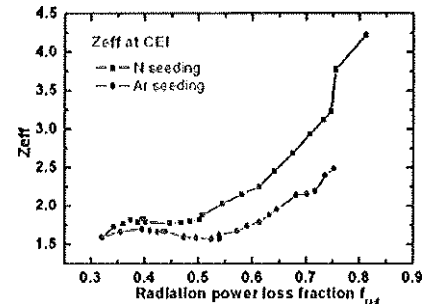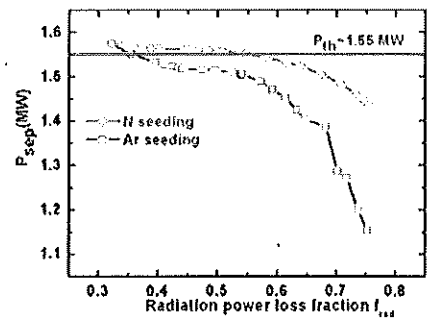
tokamaks to the level of C wall observed in ASDEX-U and JET [4, 14].

4. Conclusions

We have simulated an L-mode double null discharge with N and Ar seeding from lower dome. The simulations indicate that both N and Ar puffing can effectively reduce the peak heat flux load and electron temperature Te at divertor targets similarly. N seeding can reach a higher radiative loss fraction (~85%) than Ar case (~75%), and N radiates power in divertor region mianly, while the radiative power inside separatrix for Ar seeding is also significant. The maximum radiation power loss fraction f_{rad} ($=P_{rad,tot}/P_{in}$) ~85% in N seeding is higher than in Ar case with f_{rad}~75%. N radiates power in divertor region mianly, while the radiative power inside separatrix for Ar seeding is also significant. For both N and Ar seeding, the radiation ratio of edge to core region increases as the total radiation increasing, and reach the max value and then the radiation region move into the separatrix. The divertor get detachment when the impurity

FIG 6. The radiative power loss rate L_z of some important elements in tokamak as a function of temperature at a fixed ne.

gas puffing reach a high level for both N and Ar seeding. We also found that Z_{eff} at CEI is totally larger in N seeding than in Ar seeding at a fixed f_{rad}, and Ar impurity puffing results in a faster decrease of P_{sep} than N. Those indicate that Ar may be not a good radiator for confinement with the heating power close to the L-H transition threshold. It seems N is well suited and even better than Ar for current discharge parameters. This may because that the majority of radiative peak for N is at lower temperature which corresponds to divertor region. Further studies of the compatibility and mechanism of high confinement with impurity seeding will be performed to optimize the choice of radiators.
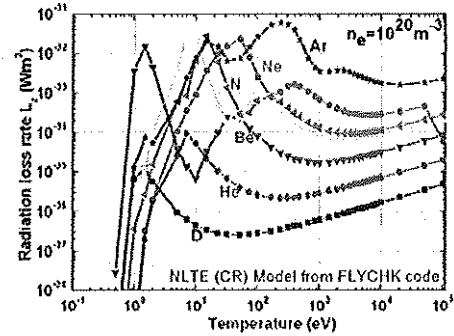
Acknowledgements

References
[1] G. Janeschitz, et al., Nucl. Fusion 42, 14 (2002)
[2] M. L. Reinke, J. W. Hughes, A. Loarte, D. Brunner, I. H. Hutchinson et al., J. Nucl. Mater. 415, S340 (2011)
[3] G. L. Jackson, M. Murakami, D. R. Baker, R. Budny et al., Plasma Phys. Control. Fusion 44,1893 (2002)
[4] J. Schweinzer, A. C. C. Sips, G. Tardini, P. A. Schneider et al., Nucl. Fusion 51, 113003 (2011)
[5] A. Kallenbach, M. Bernert, R. Dux, L. Casali, T. Eich et al., Plasma Phys. Control. Fusion 55,124041 (2013)
[6] R. Schneider, X. Bonnin, K.Borras, D. P. Coster et al., Contrib. Plasma Phys. 46(1-2), 3-191 (2006)
[7] D. Reiter, M. Baelmans, P. Börner, Fusion Science and Technology. 47(2), 172-186 (2005)
[8] H. P. Summers, http://www.adas.ac.uk./manual.php, 2004
[9]W. Echstein and D. B. Heifetz, J. Nucl. Mater. 145-147, 332(1987)
[10] S. K. Rathgeber, R. Fischer, S. Fietz, A. Kallenbach et al, Plasma Phys. Control. Fusion 52,095008 (2010)
[11] A. Loarte, J. W. Hughes, M. L. Reinke, J. L. Terry et al, Phys. Plasmas 18,056105 (2011)
[12] C. B. Huang, X. Gao, Z. Liu, X. Han, T. Zhang et al, Plasma Phys. Control. Fusion 52,075005 (2016)
[13] http://adas.phys.strath.ac.uk/.
[14] C. Giround, G. P. Maddison, S. Jachmich, F. Rimini et al, Nucl. Fusion 53,113025 (2013)